Tungsten(VI) Oxide Flake-Wall Film Electrodes for Photoelectrochemical Oxygen Evolution from Water

Fumiaki Amano, Ding Li and Bunsho Ohtani

ECS Trans. 2010, Volume 28, Issue 17, Pages 127-133.
doi: 10.1149/1.3503359

ECS Transactions, 28 (17) 127-133 (2010)
10.1149/1.3503359 ©The Electrochemical Society

Tungsten(VI) Oxide Flake-Wall Film Electrodes for Photoelectrochemical Oxygen Evolution from Water

F. Amano[ab], D. Li[b], and B. Ohtani[ab]

[a] Catalysis Research Center, Hokkaido University, Sapporo 001-0021, JAPAN
[b] Graduate School of Environmental Science, Hokkaido University, Sapporo 060-0810, JAPAN

A vertically arrayed flake film, "flake-wall film", of monoclinic tungsten(VI) oxide (WO_3) was prepared on a transparent conductive glass. The WO_3 flake-wall film exhibited superior performance for photoelectrochemical water oxidation under visible-light irradiation compared to that of a film consisting of horizontally laminated WO_3 flakes. The small difference between photocurrent densities under front-side irradiation and back-side irradiation indicates the excellent electron transport property of the flake-wall film.

Introduction

Development of highly efficient semiconductor electrodes and photocatalysts is one of the most important subjects for solar-energy conversion and environmental purification. Photoelectrochemical oxidation of water into oxygen is induced by photogenerated valence-band holes of n-type metal-oxide films under anodic polarization. High incident photon-to-current conversion efficiency has been reported for nanocrystalline films with a large interface of semiconductor/liquid (1-5). The nanocrystalline films require thickness of several micrometers to maximize absorption of incident photons, while increase in the thickness would increase the density of grain boundaries, resulting in retardation of electron transport to the back-contacted conductive substrate due to resistance (Fig. 1a) (6, 7). The grain boundaries also seem to act as recombination centers to reduce the lifetime of photoexcited carriers. On the other hand, films of plate-like crystallites vertically arrayed to the substrate are expected to exhibit photoelectrochemical performance superior to that of films with a large number of grain boundaries (Fig. 1b). Recently, we have fabricated tungsten(VI) oxide (WO_3) films consisting of crystalline flakes vertically arrayed to the substrate (flake-wall films) by controlling anisotropic crystal growth of tungsten oxide monohydrate ($WO_3 \cdot H_2O$) followed by calcination (8). In the present study, we investigated the photoelectrochemical properties of the flake-wall film for water oxidation.

Experimental

Preparation of tungsten oxide films

Tin-oxide (SnO_2)-deposited glass was used for a transparent conductive substrate and was covered with a nanocrystalline WO_3 thin film using a colloidal solution of tungstic acid. The colloidal solution was obtained by passing an aqueous solution of sodium tungstate through a column packed with a proton exchange resin (DOWEX 50WX2, 100-200 mesh), followed by collection in ethanol and evaporation to give a solution with a concentration of ca. 1.0 mol L^{-1}. After addition of polyethylene glycol 300 (Wako Pure

Chemical Industries), the viscous colloidal solution was coated on a conductive glass by a paste-squeegee method and annealed at 773 K for 30 min.

Deposition of $WO_3 \cdot H_2O$ crystallites was performed using a newly developed solvothermal method. Tungsten(VI) chloride (WCl_6, 2 mmol) was dissolved in 70 mL ethanol in a globe box filled with dry air to prevent hydrolysis by atmospheric humidity. The substrate covered with a nanocrystalline WO_3 film (5.25 cm^2) was immersed in the ethanol solution of WCl_6 and heated in a 100-mL Teflon-lined autoclave at 373 K for 20 h. The obtained film was washed with water, dried at 393 K, and calcined at 773 K for 2 h.

Another film consisting of horizontally laminated flakes (flake-laminate films) was prepared by a paste-squeegee method using $WO_3 \cdot H_2O$ precipitates crystallized during the solvothermal reaction for the flake-wall film preparation. The paste obtained by mixing crystalline powders, pure water, acethylacetone, and surfactant Toriton X-100 (Aldrich) in a mortar was coated on the SnO_2 glass or nanocrystalline WO_3 film, followed by calcination at 773 K for 2 h.

Photoelectrochemical reaction

The photoelectrochemical properties of the prepared films were investigated using a three-electrode system in a cylindrical glass vessel at room temperature. A platinum wire was used as a counter electrode. A silver/silver chloride (Ag/AgCl) electrode in an aqueous solution of 3 mol L^{-1} sodium chloride (+0.209 V vs. SHE) was used as a reference electrode. An aqueous solution of 0.1 mol L^{-1} sodium sulfate (Na_2SO_4) was used as a supporting electrolyte. The electrode potential was swept in the anodic direction at a rate of 50 mV s^{-1} using a potentiostat (Princeton Applied Research PARSTAT 2263). Visible light irradiation (> 400 nm) was performed using a 300-W xenon arc lamp equipped with a cut-off filter (Asahi Techno Glass L42) under magnetic stirring.

Characterization

Scanning electron microscopic (SEM) images were obtained by a JEOL JSM-7400F. Diffuse transmission spectra were recorded by a JASCO V-670 spectrometer equipped with a PIN-757 integrating sphere. X-Ray diffraction (XRD) patterns were recorded on a Rigaku RINT ULTIMA diffractometer with Cu K_α radiation.

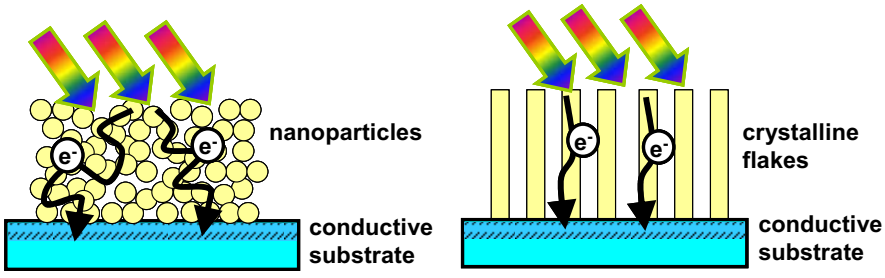

Figure 1. Schematic illustration of photoexcited electron transport in a nanocrystalline film and a vertically arrayed crystalline film.

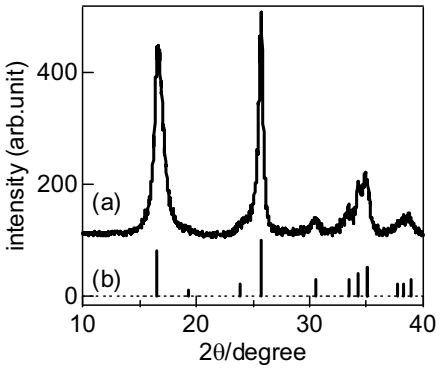

Figure 2. XRD patterns of (a) particles generated by solvothermal reaction and (b) $WO_3 \cdot H_2O$ (JCPDS card no. 43-0679).

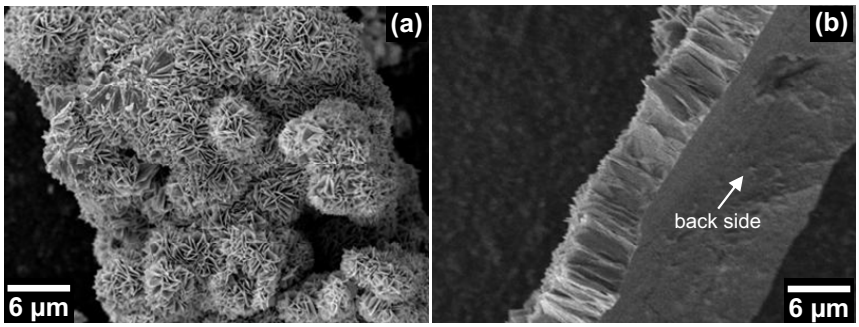

Figure 3. SEM images of particles collected from (a) the bottom and (b) the wall of the Teflon-lined autoclave after solvothermal reaction.

Results and Discussion

Flake-wall film

XRD pattern and SEM images of the precipitates generated by solvothermal reaction of WCl_6 in ethanol solution are shown in Figures 2 and 3, respectively. The particles exhibited XRD pattern attributable to crystalline $WO_3 \cdot H_2O$ (JCPDS card no. 43-0679). The morphology of particles was found to be micrometer-sized aggregates composed of many crystalline flakes. Some precipitates weakly deposited on the wall of the Teflon-lined autoclave showed arrays of crystalline flakes (Fig 1b). This self-arrayed crystal growth would occur after heterogeneous nucleation on the wall.

Based on the findings of production of flake arrays, we tried to control the self-arrayed anisotropic crystal growth of $WO_3 \cdot H_2O$ on a transparent conductive substrate. Covering with a nanocrystalline WO_3 film was found to be essential for fabricating a vertically oriented flake film. No appreciable deposition was observed on a substrate in the absence of a nanocrystalline WO_3 film, which was assumed to be a base layer for heterogeneous nucleation and adhesion of crystalline $WO_3 \cdot H_2O$ on the substrate. It should be noted that the base layer plays a role of protection from damage by strong acidity of the solution. The thus-obtained film was calcined in air at 773 K for 2 h.

Figure 4 shows side-view and top-view SEM images of the prepared film. Crystalline flakes with heights of several micrometers were seen to be self-arrayed and normal to the substrate covered by a nanocrystalline WO_3 film with a height of ca. 1 μm. This film was called as a WO_3 flake-wall film, because the crystalline flakes were vertically standing on the substrate like a wall. XRD measurement suggests that most of the (110) planes of monoclinic WO_3 were parallel to the substrate (8).

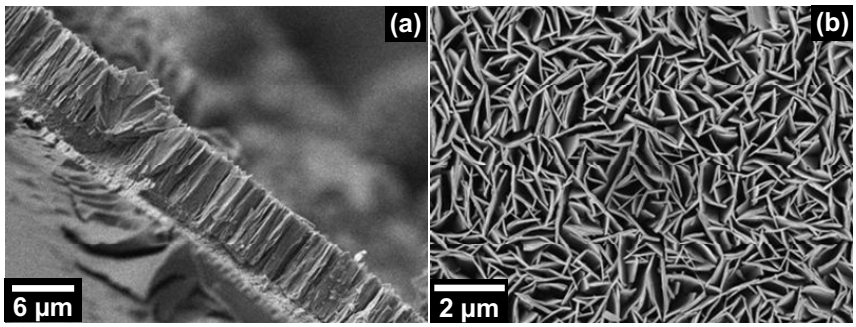

Figure 4. (a) Side-view and (b) top-view images of a flake-wall film.

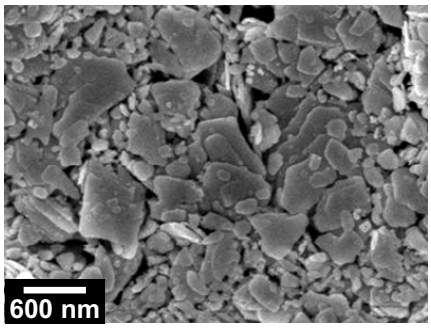

Figure 5. Top-view SEM images of a flake-laminate film.

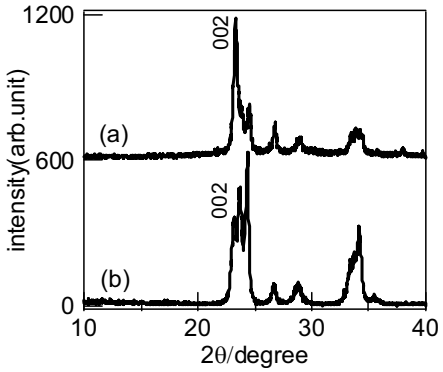

Figure 6. XRD patterns of (a) a flake-laminate film on SnO_2 glass and (b) WO_3 particles prepared by calcination of $WO_3 \cdot H_2O$ particles.

TABLE I. Amount of WO_3 on the films and ratio of photocurrent density (*I*) by front-side irradiation to that by back-side irradiation.

sample	weight of nanocrystalline WO_3 film/mg	total weight of WO_3/mg	ratio of *I*(front side) to *I*(back side)
flake-wall film	2.1	8.6	0.7
laminate film	2.2	8.2	0.2

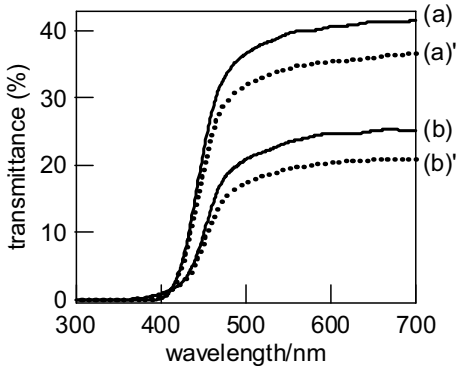

Figure 7. Diffuse transmittance spectra of (a) a flake-wall film and (b) a flake-laminate film. The films were illuminated from (solid curve) the back side and (dotted curve) the front side.

Flake-laminate film

Figure 5 shows top-view SEM images of another film prepared by a paste-squeegee method using $WO_3 \cdot H_2O$ precipitates and subsequent calcination. The crystalline flakes were found to be piled up on the substrate. Figure 6 shows XRD patterns of the film and the calcined powder of $WO_3 \cdot H_2O$ precipitates. Both patterns could be assigned to monoclinic WO_3. The peak intensity of 002 diffraction for the film was found to be much higher than that for the particles. This indicates that the (001) planes of monoclinic WO_3 have a tendency to be parallel to the substrate. Considering the preferential orientation of the (110) planes parallel to the substrate in the case of a flake-wall film (8), we concluded that the largely exposed facet of crystalline flakes was WO_3 (001). This film, composed of horizontally laminated flakes, was denoted as a flake-laminate film.

Photoelectrochemical properties

Photoelectrochemical water oxidation was performed in an aqueous solution of 0.1 mol L^{-1} Na_2SO_4 under visible light irradiation. In order to compare the photoelectrochemical properties of flake-wall and flake-laminate films, we prepared films with similar weights of WO_3. Since a base layer of nanocrystalline film is necessary for fabrication of a flake-wall film, the flake-laminate film was prepared on the nanocrystalline film deposited on the SnO_2 glass. The amounts of nanocrystalline WO_3 (and total amounts of WO_3) in those films were adjusted to similar weights as shown in Table 1. Figure 7 shows diffuse transmittance spectra of those films. The

photoabsorption edges were located at around 470 nm. Transmittance at a longer wavelength of the flake-wall film was higher than that of the laminate film, suggesting higher transparency of the flake-wall film. The transmittance of both films was dependent on the direction of incident light. Transmittance under the condition of back-side incidence through the transparent conductive glass was higher than that under the condition of front-side incidence through crystalline flakes. In the case of back-side incidence, the nanocrystalline film as a base layer might play the role of an anti-reflecting layer to diffuse light, which comes through the transparent conductive glass.

Figure 8A shows potential-current curves for the films under back-side irradiation through the transparent conductive substrate. The photocurrent of the flake-laminate film was relatively small and quickly became saturated at a low anodic potential (ca. 0.6 V vs. Ag/AgCl) compared to that of the flake-wall film. The saturated photocurrent density of the flake-wall films was much higher than that of the flake-laminate film. Figure 8B shows potential-current curves under the condition of front-side irradiation through the WO_3 layer. The photocurrent of the flake-laminate film was much smaller than that of the flake-wall film. The ratios of photocurrent density by front-side irradiation to that by back-side irradiation were found to be 0.7 for the flake-wall film and 0.2 for the flake-laminate film as shown in Table 1. This dependence of photocurrents on illumination direction indicates the presence of photoexcited carrier recombination during electron transport to the back-contacted conductive substrate. Most of the photoexcited electrons generated near the front side are not transported to the back-contacted substrate in the flake-laminate film with a high density of grain boundaries (Figure 9). On the other hand, efficient transportation of photoexcited electrons would be achieved in the flake-wall films (Figure 9). The crystallinities of flakes seem to be similar in the two films, since the conditions for growth of $WO_3 \bullet H_2O$ flakes and the calcination conditions were the same. Therefore, the difference in transport of photoexcited electrons would be due only to the orientation of the flake-like crystalline nanostructure to the substrate. It is concluded that the high efficiency of a flake-wall film for photoelectrochemical oxidation of water is probably due to the low density of grain boundaries in the electron-transport direction.

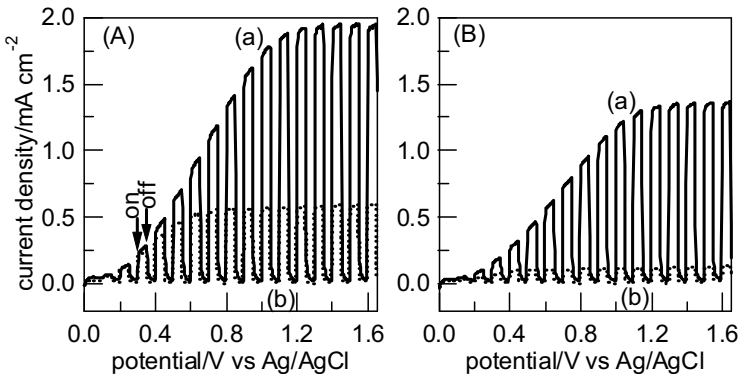

Figure 8. Current-potential plots for (a) a flake-wall film and (b) a flake-laminate film in an aqueous solution of 0.1 mol L^{-1} Na_2SO_4 under chopped visible-light irradiation. The films were illuminated from (A) the back side and (B) the front side.

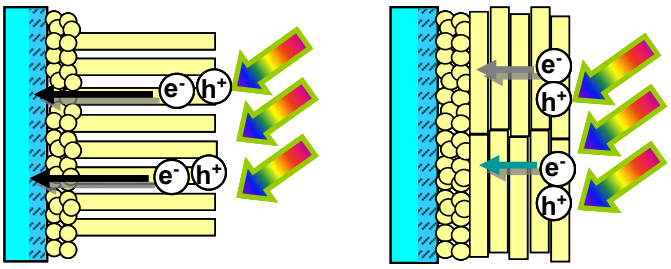

Figure 9. Schematic illustration of photoexcited electron transport in a flake-wall film and in a flake-laminate film under front-side irradiation.

Conclusion

WO_3 flake-wall films exhibited photoelectrochemical efficiency higher than that of flake-laminate films. Since the crystallinity of flakes seems to be similar in these films, the difference in photoactivities would be due to orientation of plate-like crystallites to the substrate; the flake-wall film exhibits a lower density of grain boundaries in the electron-transport direction. This would be the reason for the higher efficiency for photoelectrochemical oxidation of water compared to films with a high density of grain boundaries.

Acknowledgments

This work was supported in part by the Global COE Program (Project No. B01: Catalysis as the Basis for Innovation in Materials Science) from the Ministry of Education, Culture, Sports, Science and Technology, Japan (MEXT). FA is grateful to Nissan Science Foundation, Japan for financial support. SEM measurements were supported by Hokkaido Innovation through Nanotechnology Support (HINTS) of MEXT.

References

1. C. Santato, M. Odziemkowski, M. Ulmann and J. Augustynski, *J. Am. Chem. Soc.*, **123**, 10639 (2001).
2. C. Santato, M. Ulmann and J. Augustynski, *J. Phys. Chem. B*, **105**, 936 (2001).
3. B. Yang, Y. J. Zhang, E. Drabarek, P. R. F. Barnes and V. Luca, *Chem. Mater.*, **19**, 5664 (2007).
4. B. Yang, P. R. F. Barnes, W. Bertram and V. Luca, *J. Mater. Chem.*, **17**, 2722 (2007).
5. M. Yagi, S. Maruyama, K. Sone, K. Nagai and T. Norimatsu, *J. Solid State Chem.*, **181**, 175, (2008).
6. E. Thimsen, N. Rastgar and P. Biswas, *J. Phys. Chem. C*, **112**, 4134 (2008).
7. N. S. Gaikwad, G. Waldner, A. Bruger, A. Belaidi, S. M. Chaqour and M. Neumann-Spallart, *J. Electrochem. Soc.*, **152**, G411 (2005).
8. F. Amano, D. Li, B. Ohtani, *Chem. Commun.*, **46**, 2769 (2010).